JP1.2 Clear-Sky and Surface Narrowband Albedo Datasets Derived from MODIS Data

Yan Chen, Sunny Sun-Mack, Robert F. Arduini, and Qing Trepte
Science Systems and Applications, Inc., Hampton, VA

Patrick Minnis*
NASA Langley Research Center, Hampton, VA

ABSTRACT

Satellite remote sensing of clouds requires an accurate estimate of the clear-sky reflectance for a given scene for detecting clouds and aerosols and for retrieving their microphysical properties. Knowing the spatial and angular variability of clear-sky albedo is essential for predicting the clear-sky radiance at solar wavelengths. The Clouds and Earth's Radiant Energy System (CERES) Project uses the near-infrared (NIR; 1.24, 1.6 or 2.13 μm) channels and the visible (VIS; 0.63, 0.83 μm) available on Terra and Aqua satellites as the CERES scanners. Generally, clear-sky albedo for a given surface type is determined for conditions when the vegetation is either thriving or dormant and free of snow. The surface albedos are derived using a radiative transfer parameterization of the impact of the atmosphere, including aerosols, on the observed reflectances. This paper presents a method of generating monthly clear-sky overhead albedo maps for both snow-free and snow-covered surfaces of 1.24 μm channel using of MODIS (Moderate Resolution Imaging Spectroradiometer) CERES products. These maps will be used as the background to determine the variations in clear-sky top-of-atmosphere (TOA) albedos.

1. INTRODUCTION

To detect clouds and aerosols and retrieve their microphysical properties from satellite data, it is necessary to have an accurate estimate of the clear-sky reflectance for any given scene. Knowing the spatial and angular variability of clear-sky albedo is essential for predicting the clear-sky radiance at solar wavelengths. The Clouds and the Earth's Radiant Energy System (CERES) Project uses the visible (VIS; 0.63 μm) and near-infrared (NIR; 1.6 or 2.13 μm) channels available on the same satellites as the CERES scanners. Clear-sky albedo for a given surface type is determined for conditions when the vegetation is either thriving or dormant and free of snow. Snow albedo is typically estimated without considering the underlying surface type. The albedo for a surface blanketed by snow, however, should vary with surface type because the vegetation often emerges from the snow to varying degrees depending on the vertical dimensions of the vegetation. Accounting for vegetation effects should improve the capabilities for distinguishing snow and clouds over different surface types and facilitate improvements in the accuracy of radiative transfer calculations between the snow-covered surface and the atmosphere, eventually leading to improvements in models of the energy budgets over land at the top of the atmosphere. In the CERES Edition 3 processing, the 1.24-μm channel will also be used for retrievals over snow-covered surfaces. This paper introduces a revised method to generate monthly clear-sky overhead albedo maps for snow-free and snow-cover surfaces with a focus on 1.24-μm data.

*Corresponding author address:
Patrick Minnis, MS 420 NASA Langley Res. Ctr.,
Hampton, VA 23681
E-mail: Patrick.Minnis-1@nasa.gov

2. DATA AND METHODOLOGY

This study uses four seasonal months of *Terra* MODIS from July 2007 and *Aqua* MODIS from April, October, and December 2007. For CERES, every three out of four 1-km MODIS pixels and every other scan line are skipped to minimize processing time and data storage. Each MODIS pixel is first classified as clear or cloudy using updated versions of the CERES classification schemes (Minnis et al., 2008; Trepte et al., 2002). The radiances are compared with predicted clear-sky radiances based on empirical estimates of spectral clear-sky albedo and on skin temperatures from the Global Modeling Assimilation Office GEOS 4.03 (DAO, 1997) reanalyses adjusted using empirical estimates of spectral surface emissivity (Chen et al. 2002) and atmospheric absorption calculated with the GEOS vertical profiles of temperature and humidity.

In order to create the solar-zenith-angle (SZA) dependent directional models (DRMs), instantaneous TOA albedos of each clear pixel are first calculated. The observed clear-sky reflectance for each clear pixel is

$$\rho_\lambda = \rho_\lambda(K; LAT, LON; \mu_o, \mu, \psi) \quad (1)$$

where λ is the wavelength, K is the International IGBP surface type (see Table 1), LAT and LON are the center latitude and longitude of each pixel, respectively, μ_o are the cosines of SZA and viewing zenith angle (VZA), respectively, and ψ is the relative azimuth angle.

Each reflectance is converted to albedo α_λ in the following manner,

$$\alpha_\lambda = \rho_\lambda (K; LAT, LON; \mu_o, \mu, \psi) / \chi_\lambda(K; \mu_o, \mu, \psi), \quad (2)$$

where χ_λ is the normalized bidirectional reflectance distribution function (BRDF) for the particular surface type and wavelength. Over water surfaces, the BRDF values for all wavelengths are taken from an empirical model based on geostationary satellite data (Minnis and Harrison, 1984). A broadband empirical model (Suttles

Table 1: IGBP surface type, *K*, categories

1. evergreen needleleaf = conifer
2. evergreen broadleaf = conifer
3. deciduous needleleaf = deciduous
4. deciduous broadleaf = deciduous
5. mixed forests = 1/2 conifer + 1/2 deciduous
6. closed shrublands = mosaic
7. open shrubland = mosaic
8. woody savannas = grass
9. savannas = grass
10. grasslands = grass
11. permanent wetlands = 1/2 grass + 1/2 water
12. croplands = grass
13. urban = black body
14. mosaic = 1/2 grass + 1/2 mixed forest
15. snow/ice
16. barren/sparsely vegetated = desert
17. water
18. tundra = frost
19. coastline = 10% to 90% water

et al., 1988) is used for all wavelengths over barren desert scenes. The snow BRDFs for each wavelength are developed from a blend of calculations using an adding-doubling radiative transfer model and from snow-free observations. The snow surface is assumed to be a layer of randomly oriented, hexagonal ice crystals having a length-to-width ratio of 750μm/160μm with an optical depth of 1000 (Takano et al., 1989). The pure snow model BRDFs at the top of the atmosphere were computed using a radiative transfer model incorporating the May 22 (clear-sky) Arctic atmosphere from the European Center for Medium-Range Weather Forecasting analysis and a correlated *k*-distribution method (Kratz, 1995). The snow BRDFs were used by Chen et al. (2006) for permanent ice/snow surfaces and any other scene classified as snow covered. An empirical coastal model was used at all wavelengths for K = 19. The broadband empirical land model of Suttles et al. (1988) was used for the VIS channel over all remaining surface types (K = 1-14, 18). BRDFs for the other channels and remaining surface types were derived from aircraft measurements taken at 0.877, 1.66, and 2.13 μm for four distinct surfaces (Kriebel et al., 1978). The coniferous forest models were used for all forest types (K = 1,5), while bog was used for K = 11, 18, and 19. Savanna data were used for K = 6, 7, 8, 9, and 13 and pasture results were used for K = 10, 12, and 14.

Instantaneous TOA albedos for each pixel were then averaged for every 10 degree interval to determine the SZA dependence. The means for the 19 IGBP types were further averaged into the four Kriebel types. The DRMs of clear-sky snow-free and snow-cover albedo were then created based on the CERES algorithms and Snow & Ice Maps by NESDIS Interactive Multisensor Snow and Ice Mapping System Daily Northern and Southern Hemisphere Snow and Ice Analysis in the vicinity of coastlines in 10' grid. To improve the repre-

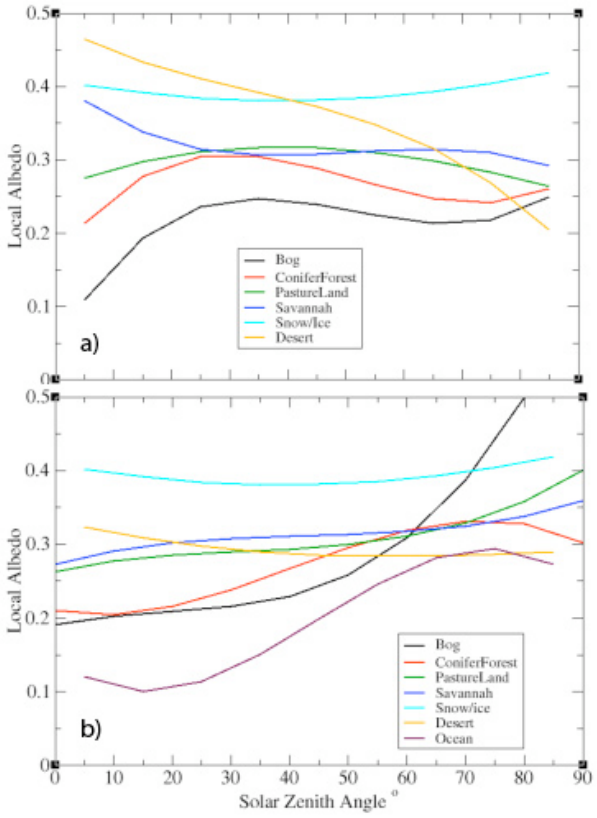

Fig. 1. Directional models for a) snow-free + permanent snow land and with b) snow-cover.

sentation of snow reflectance over vegetated areas, hybrid DRMs and BRDFs models were created. For snow-covered surfaces, we assume that the directional albedo can be expressed as a linear sum of permanent snow and snow-free surface albedos. The factor $f_{\lambda,hybrid}$ relating the two is given by

$$f_{\lambda,hybrid} = (\alpha_{\lambda,snow} - \alpha_{\lambda,perm}) /(\alpha_{\lambda,free} - \alpha_{\lambda,perm}) \qquad (3)$$

where $\alpha_{\lambda,snow}$, albedo of fresh snow over vegetated area; $\alpha_{\lambda,free}$, snow-free albedo; and $\alpha_{\lambda,perm}$, permanent snow albedo are obtained from CERES Edition MODIS products. This factor is then used to create the hybrid reflectance fields for snow-covered surfaces as linear combinations of the snow-free and permanent snow reflectances

$$\rho_{\lambda,hybrid} = f_{\lambda,hybrid}\,\rho_{\lambda,free} + (1 - f_{\lambda,hybrid})\rho_{\lambda,perm}. \qquad (4)$$

The hybrid BRDFs are then given by

$$\chi_{\lambda,hybrid} = \rho_{\lambda,hybrid} / \alpha_{\lambda,snow}. \qquad (5)$$

All clear pixels during an overpass are averaged into the appropriate 10' region, which is assigned a single surface type K defined by the International Geosphere Biosphere Programme (IGBP). The mean TOA overhead clear-sky albedo α_o for each region was computed from the observed reflectances from MODIS and the relevant DRMs and BRDFs. The four seasonal

clear-sky overhead albedo monthly maps are created based on this method.

Table 2: Seasonal IGBP average clear-sky snow-free overhead albedos

IGBP	Spring	Summer	Fall	Winter
1.	0.1442	0.1928	0.1822	0.1742
2.	0.2259	0.2263	0.2307	0.2254
3.	0.1397	0.2109	0.1783	0.2011
4.	0.1944	0.2461	0.2237	0.2146
5.	0.1505	0.2055	0.1846	0.1913
6.	0.3305	0.3549	0.3355	0.3376
7.	0.3966	0.3946	0.3951	0.4049
8.	0.3232	0.3546	0.3373	0.3317
9.	0.3689	0.3787	0.3652	0.3741
10.	0.2658	0.2847	0.2769	0.2858
11.	0.0869	0.1317	0.1332	0.1191
12.	0.2421	0.2772	0.2569	0.2506
13.	0.3012	0.3372	0.3200	0.3090
14.	0.2393	0.2753	0.2541	0.2504
15	0.4034	0.4180	0.4445	0.4062
16.	0.5156	0.4941	0.5820	0.6360
17.	0.0326	0.0326	0.0326	0.0326
18.	0.1217	0.1362	0.1422	0.1259
19.	0.1018	0.1115	0.1046	0.1055

3. RESULTS and FUTURE WORK

Figure 1 shows the SZA dependence of the 1.24 μm local albedos of snow-free (a) and snow-cover (b) for the four Kriebel types, desert (K = 16), ocean, and permanent snow (K = 15). The IGBP surface-type seasonally averaged clear-sky overhead albedos for snow-free are presented in Table 2. These averages are used to fill in the global 10' grid where observed values are absent. Figures 2 and 3, respectively, show the preliminary four seasonal clear-sky overhead 1.24-μm albedo maps with snow-free and snow-cover separately.

The brightest snow-free surfaces are found over the deserts. Some values exceed 0.70 over parts of the Sahara Desert (Fig. 2). The greatest snow albedos are found over Greenland during springtime and over Antarctica during the fall. When snow is added to the other areas (Fig. 3), the 1.24-μm albedos often decrease. Obviously, most of these areas, e.g., Sahara Desert or Amazon Basin, will never have snow, so the values are simply filled in from mid-latitude observations. They are presented here simply to have complete set of values. Because the 1.24-μm albedos for snow-covered surfaces are relatively low and comparable to their snow-free counterparts, they should be valuable for retrieving cloud optical depth over snow-covered surfaces. CERES Edition 2 used the 1.6 and 2.13-μm channels to retrieve cloud optical depth over snow from Terra and Aqua data, respectively (Minnis et al., 2010) because of the failed Aqua MODIS 1.6-μm channel. The 2.13-mm channel can only be used for a limited range of optical depths, especially for ice clouds. Thus, to maximize the range of retrieved optical depths and to maintain spectral consistency between the CERES Terra and Aqua retrievals, the 1.24 μm will be employed in future CERES analyses.

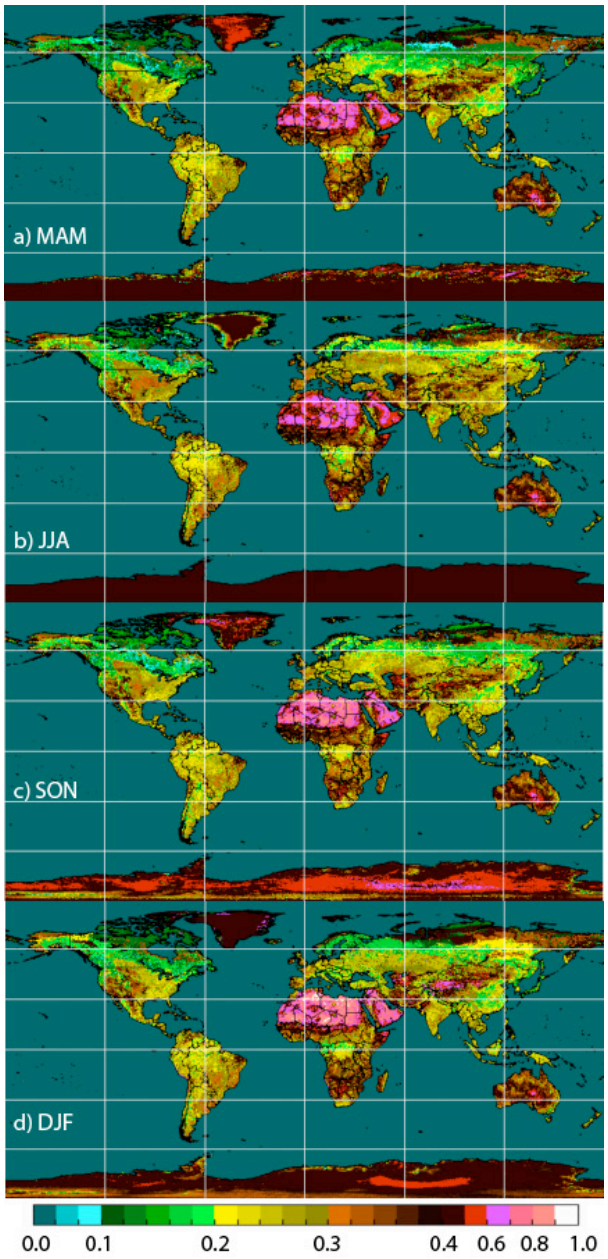

Fig. 2. Clear-sky overhead 1.24-μm albedos for snow-free and permanent snow scenes.

The clear-sky maps of 1.24 μm overhead albedo will be validated and used as the background for CERES Edition-3 cloud retrievals. Clear-sky overhead albedo maps were created for the MODIS 0.63, 0.83, 1.6, and 2.13-μm channels by Chen et al. (2006) using an older technique. They will be updated using the methods described here, specifically, by applying hybrid snow-vegetation bidirectional reflectance models.

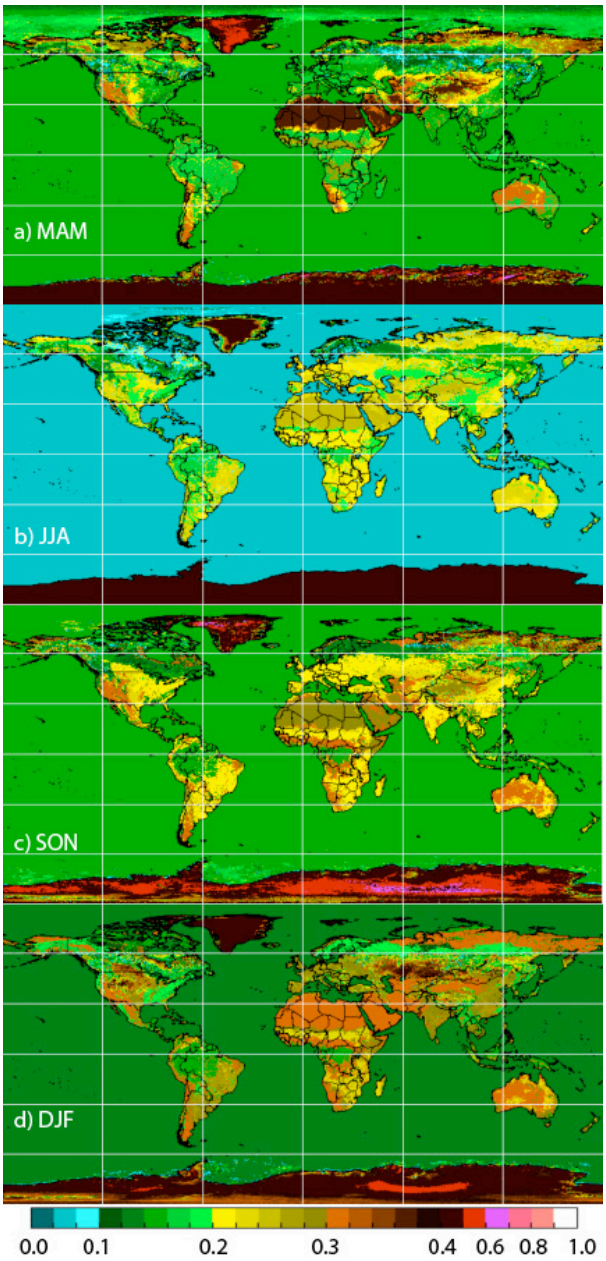

Fig. 3. Clear-sky overhead 1.24-μm albedos for snow-covered scenes.

4. REFERENCES

Chen, Y., P. Minnis, S. Sun-Mack, and R. F. Arduini, 2006: Clear-sky and surface narrowband albedo variations derived from VIRS and MODIS data. *Proc. AMS 12th Conf. Atmos. Radiation. Madison*, WI, July 10-14, CD-ROM, 5.6.

Chen, Y., S. Sun-Mack, P. Minnis, D. F. Young, and W. L. Smith, Jr., 2002: Surface spectral emissivity derived from MODIS data. *Proc. SPIE Conf. Optical Remote Sensing of Atmos. and Clouds III*, Hangzhou, China, Oct. 23-27, **4891**, 361-369.

DAO, 1997: GEOS-3 Data Assimilation System Architectural Design. *DAO Office Note 97-06*. Data Assimilation Office, Goddard Space Flight Center, Greenbelt, MD 20771.

Kratz, D.P., 1995: The correlated-k distribution technique as applied to the AVHRR channels. *J. Quant. Spectrosc. Radiat. Transfer*, **53**, 501-510.

Kriebel, K. T., 1978: Measured spectral bidirectional reflectance properties of vegetated surfaces. *Appl. Opt.*, **17**, 253-259.

Minnis, P. and E. F. Harrison, 1984: Diurnal variability of regional cloud and clear-sky radiative parameters derived from GOES data. Part III: November 1978 radiative parameters. *J. Climate Appl. Meteor.*, **23**, 1032-1051.

Minnis, P., and co-authors, 2008: Cloud detection in non-polar regions for CERES using TRMM VIRS and Terra and Aqua MODIS data. *IEEE Trans. Geosci. Remote Sens.*, **46**, 3857-3884

Minnis, P., and Co-authors, 2010: CERES Edition-2 cloud property retrievals using TRMM VIRS and Terra and Aqua MODIS data, Part I: Algorithms. Submitted to *IEEE Trans. Geosci. Remote Sens.*

Suttles, J. T., R. N. Green, P. Minnis, G. L. Smith, W. F. Staylor, B. A. Wielicki, I. Walker, D. F. Young, V. R. Taylor, and L. L. Stowe, 1988: Angular radiation models for Earth-atmosphere system, Vol. 1, Shortwave radiation. *NASA RP-1184*, 144 pp.

Takano, Y. and K. N. Liou, 1989: Radiative transfer in cirrus clouds: I single scattering and optical properties of oriented hexagonal ice crystals. *J. Atmos. Sci.*, **46**, 3-20.

Trepte, Q. Z., P. Minnis, and R. F. Arduini, 2002: Daytime and nighttime polar cloud and snow identification using MODIS. *Proc. SPIE Conf. Optical Remote Sensing of Atmos. and Clouds III*, Hangzhou, China, Oct. 23-27, **4891**, 449-459.